Published in final edited form as:
Inorg Chem. 2008 August 18; 47(16): 7405–7414. doi:10.1021/ic8007552.

Redox and Structural Properties of Mixed-Valence Models for the Active Site of the [FeFe]-Hydrogenase: Progress and Challenges

Aaron K. Justice, **Luca De Gioia**, **Mark J. Nilges**, **Thomas B. Rauchfuss**, **Scott R. Wilson**, and **Giuseppe Zampella**

Department of Chemistry, University of Illinois at Urbana-Champaign, Urbana, IL, 61801, rauchfuz@uiuc.edu Department of Biotechnology and Biosciences, University of Milano—Bicocca, Piazza della Scienza 1, 20126-Milan, Italy, luca.degioia@unimib.it

Abstract

The one-electron oxidations of a series of diiron(I) dithiolato carbonyls were examined to evaluate the factors that affect the oxidation state assignments, structures, and reactivity of these low-molecular weight models for the H_{ox} state of the [FeFe]-hydrogenases. The propanedithiolates $Fe_2(S_2C_3H_6)(CO)_3(L)(dppv)$ (L = CO, PMe_3, P*i*-Pr_3) oxidize at potentials ~180 mV milder than the related ethanedithiolates (*Angew. Chem. Int. Ed.* **2007**, *46*, 6152). The steric clash between the central methylene of the propanedithiolate and the phosphine favors the rotated structure, which forms upon oxidation. EPR spectra for the mixed-valence cations indicate that the unpaired electron is localized on the Fe(CO)(dppv) center in both $[Fe_2(S_2C_3H_6)(CO)_4(dppv)]BF_4$ and $[Fe_2(S_2C_3H_6)(CO)_3(PMe_3)(dppv)]BF_4$, as seen previously for the ethanedithiolate $[Fe_2(S_2C_2H_4)(CO)_3(PMe_3)(dppv)]BF_4$. For $[Fe_2(S_2C_nH_{2n})(CO)_3(P\textit{i}\text{-}Pr_3)(dppv)]BF_4$, however, the spin is localized on the Fe$(CO)_2(P\textit{i}\text{-}Pr_3)$ center, although the Fe(CO)(dppv) site is rotated in the crystalline state. IR and EPR spectra, as well as redox potentials and DFT-calculations, suggest, however, that the Fe$(CO)_2(P\textit{i}\text{-}Pr_3)$ site is rotated in solution, driven by steric factors. Analysis of the DFT-computed partial atomic charges for the mixed-valence species shows that the Fe atom featuring a vacant apical coordination position is an electrophilic Fe(I) center. One-electron oxidation of $[Fe_2(S_2C_2H_4)(CN)(CO)_3(dppv)]^-$ resulted in 2e oxidation of 0.5 equiv to give the μ-cyano derivative $[Fe^I{}_2(S_2C_2H_4)(CO)_3(dppv)](\mu\text{-}CN)[Fe^{II}{}_2(S_2C_2H_4)(\mu\text{-}CO)(CO)_2(CN)(dppv)]$, which was characterized spectroscopically.

Introduction

Modeling of the diiron active site of the [FeFe]-hydrogenases has provided a rich and tractable set of challenges to organometallic chemistry.[1] Motivated by discoveries in biophysical chemistry,[2,3] the chemistry of the $Fe_2(SR)_2(CO)_{6-x}L_x$ system, previously well examined, has been rejuvenated. Ongoing work in this and other laboratories has shown that these complexes are versatile with respect to redox, substitution, and functionalizability in ways that are pertinent to the enzyme's active site. A significant breakthrough in the modeling efforts entailed the preparation of the mixed-valence derivatives of the formula the $[Fe^IFe^{II}(SR)_2(CO)_{4-x}(PMe_3)L_x]^+$ (L = carbene or diphosphine).[4,5] These species exhibit the "rotated" stereochemistry for one of the two Fe centers (Scheme 1). This stereochemistry

Correspondence to: Luca De Gioia; Thomas B. Rauchfuss.

Supporting Information Available: Crystallographic data for $[Fe_2(S_2C_3H_6)(CO)_3(PMe_3)(dppv)]BF_4$ and $[Fe_2(S_2C_3H_6)(CO)_3(P\textit{i}\text{-}Pr_3)(dppv)]BF_4$, voltammograms, as well as IR, EPR, and NMR spectra. For DFT calculations: atomic coordinates, energy values, spin populations and partial atomic charges for the DFT models $[Fe_2(S_2C_nH_{2n})(CO)_3(PH_3)_3]^+$, $[Fe_2(S_2C_nH_{2n})(CO)_3(PMe_3)(dppv)]^+$, and $[Fe_2(S_2C_nH_{2n})(CO)_3(P\textit{i}\text{-}Pr_3)(dppv)]^+$. This material is available free of charge via the Internet at …

exposes a vacant coordination site on one Fe center, as had been anticipated by numerous biophysical studies.[2] This geometry was rare in the otherwise extensive chemistry of diiron dithiolato carbonyls.[6] Now that the rotated geometry has been demonstrated to exist in the absence of the protein, efforts can be expected to focus on the factors that govern this geometry and its reactivity.[7,8] In this work, we probe the effects of both the dithiolate and especially the terminal ligands on the electronic and molecular structure of the mixed valence state.

Modeling of the [FeFe]-hydrogenases started with the preparation of $[Fe_2(SR)_2(CN)_2(CO)_4]^{2-}$,[9] this anion being notable because it featured five of six known ligands in the active site. The redox and protonation of this dicyanide has been developed only to a limited extent.[10] Such studies are complicated by the reactivity inherent in the cyanide ligand, which is known to bridge to other metals and to protonate readily.[11] The modeling efforts have advanced significantly by using tertiary phosphine ligands in the place of the cyanides. In this paper, we return briefly to the redox chemistry of the diiron centers supported by a cyanide ligand.

Results

$[Fe_2(S_2C_3H_6)(CO)_4(dppv)]^+$

The cyclic voltammetry of the recently reported complexes[12] $Fe_2(S_2CnH_{2n})(CO)_4(dppv)$ established that the propanedithiolate (**2pdt**) undergoes oxidation at *ca*. 190 mV more cathodic than the ethanedithiolato analogue (**2edt**) (Figure 1). The redox potentials for these couples were unchanged when the oxidations were conducted under argon, dihydrogen, and dinitrogen; traces of water also had no effect.

From the CV results, the complex $Fe_2(S_2C_3H_6)(CO)_4(dppv)$, **2pdt**, was shown to undergo a one-electron oxidation at a potential less than the $Fc^{0/+}$ couple (0.5 V in CH_2Cl_2 vs Ag/AgCl).[13] This conversion was confirmed on a preparative scale by treating a CH_2Cl_2 solution of **2pdt** with $FcBF_4$ at −45 °C. The IR spectrum of the product (ν_{CO} = 2076, 2019, 1943 cm^{-1}) proved to be similar to that for the recently reported[5] $[Fe_2(S_2C_2H_4)(CO)_3(PMe_3)(dppv)]BF_4$ but shifted to higher energy by ~50 cm^{-1}, reflecting the effect of replacing PMe_3 by CO (Figure 2). Solutions of $[\mathbf{2pdt}]^+$ were found to react with NO to yield $[Fe_2(S_2C_3H_6)(CO)_3(dppv)(NO)]^+$, with the NO bound on the Fe(dppv) side of the molecule, consistent with an open coordination site residing on the Fe(dppv) (eq 1).[14]

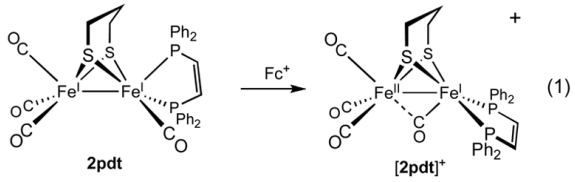

(1)

Oxidation of $Fe_2(S_2C_3H_6)(CO)_3(PMe_3)(dppv)$

In a preliminary report, we had described the one-electron oxidation of the ethanedithiolate $Fe_2(S_2C_2H_4)(CO)_3(PMe_3)(dppv)$ (**3edt**).5 Oxidation of the related propanedithiolate (**3pdt**) using $FcBF_4$ yielded the corresponding derivative $[Fe_2(S_2C_3H_6)(CO)_3(PMe_3)(dppv)]BF_4$ ($[\mathbf{3pdt}]BF_4$) but at a potential that is milder by ~180 mV. We verified the electrochemical results with a preparative scale reaction. When a 1:1 mixture of **3pdt** and **3edt** was treated with one equiv of $FcBF_4$ (0.5 equiv per diiron), we observed complete consumption of **3pdt** as indicated by the loss of the high energy ν_{CO} band, uniquely assigned to the $S_2C_3H_6$ derivative. Only upon the addition of a second equiv of $FcBF_4$ did **3edt** undergo oxidation. The structure of $[\mathbf{3pdt}]BF_4$ was confirmed crystallographically (see below). The IR spectrum (Figure 2) of

[**3pdt**]BF_4 salt was very similar to that for [**2edt**]BF_4, the greatest difference being for the $\nu_{\mu\text{-}CO}$ band which occurred at 7 cm^{-1} higher energy for the $S_2C_3H_6$ derivative.

A solution of [**3pdt**]$^+$ was found to react with CO to yield the adduct [**3pdt**CO]BF_4. Intermediates were not observed. The rate of carbonylation was slower ($t_{1/2}$ ~ 600 s at 1 atm., −45 °C) than the carbonylation of [**2edt**]$^+$ ($t_{1/2}$ ~ 30 s at 1 atm., −45 °C). The slowness of the carbonylation is attributed to the required, sluggish relocation of the PMe_3 ligand to a basal position, apparently driven by avoidance of a steric clash with the propanedithiolate strap. For diiron dithiolates bearing seven terminal ligands, it is known that the propanedithiolates (vs ethanedithiolate) tend to be less stable, which is attributable to steric congestion.[8,15] In contrast, mixed-valence complexes with a propanedithiolate are more stable than the ethanedithiolate analogues.

The stereochemistry of [**3pdt**CO]BF_4 can be assigned on the basis of its solution EPR spectrum, wherein we observed 1:4:4:1 quartet resulting from three smaller ^{31}P hyperfine couplings associated with three basal phosphine ligands. This pattern is consistent with the previously published analysis of H_{ox}^{CO} models (see below).[8] In addition to its slow formation, [**3pdt**CO]$^+$ differs from [**3edt**CO]$^+$ with respect to $\nu_{\tilde{\mu}CO}$, which is 1791 cm^{-1} in the propanedithiolate and 1783 cm^{-1} in the ethanedithiolate. The terminal ν_{CO} bands are also shifted for [**3pdt**CO]$^+$ but in the opposite fashion, reflecting a compensating relationship between $\nu_{\tilde{\mu}CO}$ and $\nu_{\square\text{-}CO}$. The binding of CO is a reversible process: an N_2 purge slowly regenerated [**3pdt**]$^+$. The EPR spectrum for [**3edt**CO]$^+$ (see below) differed from that for [**3pdt**CO]$^+$, being consistent with apical PMe_3 and dibasal dppv (Scheme 2).

$[Fe_2(S_2C_2H_4)(CO)_3(PCy_3)(dppv)]^{0/+}$

Unlike the analogous PMe_3 derivative, the tricyclohexylphosphine complex $Fe_2(S_2C_2H_4)(CO)_3(PCy_3)$(dppv) (**4edt**) could not be prepared by thermally induced substitution of **2edt**. Photochemical substitution proved efficient however. The spectroscopy for **4edt** was unremarkable, and the position of the ν_{CO} bands (ν_{CO}(avg) ~ 1927 cm^{-1}) indicated that the complex resembles **3edt**. Unexpectedly, the CV data (+140 mV vs Ag/AgCl) showed that **4edt** was more difficult to oxidize than the analogous PMe_3 derivative, which provided the first clue that the bulk of the trialkylphosphine ligands might strongly affect the electronic structure of these diiron compounds.

Oxidation of **4edt** was effected in the usual way using $FcBF_4$ at −45 °C in CH_2Cl_2. IR measurements showed that the oxidation shifts ν_{CO} by an average of ~50 cm^{-1}, as seen for the corresponding oxidations of **2pdt**, **3edt**, and **3pdt**. The average of the terminal ν_{CO} bands was, however, lower than that observed for [**3edt**]$^+$, and the pattern was distinctly different, indicating that the structures of [**3edt**]$^+$ and [**4edt**]$^+$ differ. These cations also differ in terms of their stabilities: solutions of [**3edt**]$^+$ are stable for a few seconds at room temperature, whereas the decomposition of [**4edt**]$^+$ is already apparent near −20 °C. For reasons of preparative convenience, further studies on bulky phosphines were conducted with P*i*-Pr_3 instead of PCy_3 (next section).

$[Fe_2(S_2CnH_{2n})(CO)_3(Pi\text{-}Pr_3)(dppv)]^{0/+}$

Using to the methods to obtain [**4edt**]$^+$, the complexes Fe_2(xdt)$(CO)_3$(P*i*-Pr_3)(dppv) were prepared for both xdt = **edt** and **pdt**. The IR spectra for the trisubstituted diiron(I) complexes (**4edt**, **3pdt**, **5edt**, and **5pdt**) were very similar. The ^{31}P DNMR properties for this series differed, however. The DNMR properties of **3edt** and **3pdt** have been previously discussed.[12] At 20 °C, the ^{31}P NMR spectrum of **5edt** featured both a broad and a sharp singlet, assigned respectively to the dppv ligand and P*i*-Pr_3. At −40 °C, the dppv signal decoalesced into a pair of doublets, whereas the singlet assigned to P*i*-Pr_3 remained sharp. The low barrier for

dynamics at the Fe(CO)(dppv) site is consistent, indirectly, with the location of the P*i*-Pr_3 in a basal site, which would destabilize the apical-basal spanning dppv due to a steric interaction across the two basal sites. For **5pdt**, the 20 °C ^{31}P NMR spectrum consisted of two singlets in a 2:1 ratio, again assigned to the dppv and P*i*-Pr_3 ligands, respectively. The structures of **5edt** and **5pdt**, which wasverified crystallographically, see Supporting Information) are as follows:

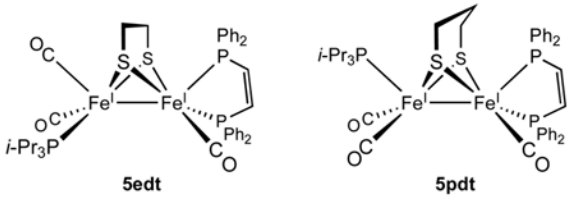

The cyclic voltammetry of CH_2Cl_2 solutions of **5edt** and **5pdt** showed that both undergo one-electron oxidations. The separation, $\Delta;E_{pdt}-E_{edt}$ (160 mV), is comparable to the difference observed for **3edt** vs **3pdt**, but the absolute values of the redox couples are strikingly different. Complex **5edt** was found to oxidize at +170 mV and **5pdt** at +10 mV (vs Ag/AgCl). These potentials are *ca.* 150 mV more anodic than seen for related **3edt** and **3pdt** (Figure 1). One-electron oxidation of **5edt** with $FcBF_4$ gave the mixed-valence salt $[Fe_2(S_2C_2H_4)(CO)_3(Pi\text{-}Pr_3)(dppv)]BF_4$, [**5edt**]$BF_4$. IR spectra in the ν_{CO} region are virtually identical for [**5edt**]$^+$ and the PCy_3-containing cation [**4edt**]$^+$. One-electron oxidation of **5pdt** at −45 °C using $FcBF_4$ afforded [**5pdt**]BF_4. Values for $\nu_{t\text{-}CO}$ for [**5pdt**]$^+$ and [**5edt**]$^+$ match closely (Figure 3). A significant difference is, however, observed for $\nu_{\mu\text{–}CO}$, which is 1830 cm^{-1} for [**5pdt**]$^+$ vs 1870 cm^{-1} for [**5edt**]$^+$, consistent with a steric interaction between the propanedithiolate and the bulky P*i*-Pr_3 ligand, which displaces the bridging CO toward a more symmetrically bridging position, as anticipated by the DFT calculations (see below, Scheme 3, see below for explanation).

Complex [**5edt**]$^+$ was found to form an adduct with CO, but the carbonylation (~30 min at −45 °C) is significantly slower than for [**3edt**]$^+$ (~30 s at −45 °C). The IR and EPR spectra of [**3edt**CO]$^+$ and [**5edt**CO]$^+$ are very similar, indicating similar structures, despite structural differences of the precursors. The average of the two ν_{tCO} bands is 20 cm^{-1} lower for [**5edt**]$^+$ vs [**3edt**]$^+$. This difference is consistent with the presence of a $Fe^{II}(CO)_2(PMe_3)$ vs a $Fe^{I}(CO)_2(Pi\text{-}Pr_3)$ site, i.e., the larger phosphine redirects the site of oxidation. A similar pattern applies also to the [**3pdt**]$^+$/[**5pdt**]$^+$ pair. Solutions of [**5pdt**]$^+$ were found to be stable at 0 °C for several minutes, whereas [**5edt**]$^+$ was found to rapidly decompose above −20 °C. Solid [**5pdt**]BF_4 was rapidly precipitated by transferring a CH_2Cl_2 solution at −45 °C into a large excess of hexane cooled to −78 °C. Although we were unable to isolate an analytically pure sample, the IR spectrum of finely powdered [**5pdt**]BF_4 (KBr pellet) matched the solution data ($\Delta;\nu_{\mu\text{–}CO}$ ~3 cm^{-1}).

Solution EPR Studies of Mixed-Valence Models

The X-band EPR spectra of frozen solutions were similar, showing axial patterns with well defined hyperfine coupling to phosphorus (Table 1). Thus, a frozen solution of [**2pdt**]BF_4 showed a triplets with $A(^{31}P)$ ~ 75 MHz, Figure 5. For the mononuclear Fe(I) complex *trans*-$[Fe(CO)_3(PPh_3)_2]^+$, the hyperfine values are ca. 55 MHz.[16] The magnitude and multiplicity of the hyperfine couplings indicate that the spin resides on the Fe(CO)(dppv) center wherein the two phosphine sites are equivalent. The EPR spectrum of the analogous salt [**3edt**]BF_4 also showed triplets with comparable *g*-values and hyperfine constants (Figure 4).

An interesting feature of the EPR spectrum of [**3pdt**]$^+$ is the presence of pairs of separate features in a ~2:1 ratio, especially discernable in the lower field signal. Each set of axial signals has a pattern (both *g* and *A* values) similar to that for [**3edt**]$^+$. The two isomers are proposed to differ with respect to the fold of the propanedithiolate. The sensitivity of the EPR spectrum to the orientation of the dithiolate backbone shows that the SOMO of [**3pdt**]$^+$ is affected by the central atom of the dithiolate (eq 2). Upon warming the solution to −50 °C, only a single isotropic triplet signal is observed.

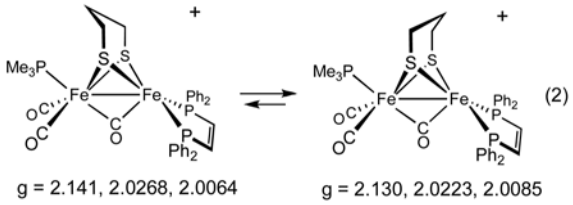

g = 2.141, 2.0268, 2.0064 g = 2.130, 2.0223, 2.0085

A similar equilibrium was not observed for other propanedithiolate derivatives, which we attribute to either (i) greater "steric asymmetry," which favors the tilting of the central methylene toward the open site on the rotated iron center ([**5pdt**]$^+$) or (ii) insensitivity of the SOMO to the asymmetry due to the presence of CO ligands in both apical positions ([**3pdt**CO]$^+$, see below).

The stereochemistry of the CO adduct, [**3pdt**CO]BF_4 was indicated by EPR spectroscopy. For such H_{ox}^{CO} models, we recently showed that phosphine ligands in the apical positions give rise to large *A*-values (>200 MHz), whereas *A*-values are much smaller (<50 MHz) for phosphine ligands attached to the basal sites.[8] For example, the EPR spectrum of [**3edt**CO]$^+$ is characterized by one large *A*-value (>250 MHz) and two smaller ones (42, 28 MHz). A very different spectrum was obtained for [**3pdt**CO]$^+$: the three $A(^{31}P)$ values were quite small (27, 39, 28, MHz; see Table 3), indicative that all three phosphine ligands occupy basal positions. Upon binding of CO, the PMe_3 undergoes a change in geometry, from apical in [**3pdt**]$^+$ to basal in [**3pdt**CO]$^+$ (Scheme 2). In general, reflecting steric crowding, the CO adducts of ethanedithiolate derivatives are significantly more stable than the propanedithiolate analogues.

Frozen solution EPR spectra of the mixed-valence P*i*-Pr_3 and PCy_3 complexes exhibit patterns with doublet features indicating that the SOMO is localized on the $Fe(CO)_2(PR_3)$ center, in contrast to the behavior of the PMe_3 complexes (Figure 5). The EPR data for [**4edt**]$^+$, [**5edt**]$^+$, and [**5pdt**]$^+$ are very similar with respect to *g* and *A* values (Table 1). The $A(^{31}P)$ values for these doublets are similar to the previously observed *A* values for the triplets seen for [**3edt**]$^+$ and [**3pdt**]$^+$. Upon warming a sample of [**5pdt**]$^+$ to −40 °C, whereupon the solvent is melts, the signal merges to give an isotropic doublet, consistent with the SOMO being localized on the $Fe(CO)_2$(P*i*-Pr_3) center.

The carbonylation of [**5edt**]$^+$ (1 atm, −45 °C) proceeded more slowly (~30 min) than for [**3edt**]$^+$, which implicates a geometric rearrangement of the phosphine ligands. The EPR spectrum of the adduct [**5edt**CO]$^+$ matched that observed for [**3edt**CO]$^+$, i.e., one large and two smaller $A(^{31}P)$ values (Table 2).

Crystallographic Characterization of $[Fe_2(S_2C_3H_6)(CO)_3(PR_3)(dppv)]BF_4$ (R = Me, *i*-Pr)

Crystals of these salts were grown at low temperatures. The [**3pdt**]$^+$ salt is unsolvated while [**5pdt**]$^+$ crystallized with a CH_2Cl_2 in the lattice; for both complexes the BF_4^- is well separated from the cationic diiron centers (Figure 6, Table 3). The cations adopt the expected structure wherein the terminal ligands on the quasi-octahedral Fe centers are staggered but that the Fe(CO)(dppv) adopts the "rotated" geometry. The CH---Fe(1) distance is 2.49 Å in [**3pdt**]BF_4,

respectively beyond the limit recognized for an agostic interaction.[17] The greater steric bulk of the $S_2C_3H_6$ vs $S_2C_2H_4$ is manifested in the rotation of the pair of phenyl groups that surround the vacant coordination site. That angle increases as follows: 4° ([**3edt**]BF_4), 14° ([**3pdt**]BF_4), and 33° ([**5pdt**]BF_4), reflecting a slightly increased tilting of the dithiolate toward the rotated Fe (the angle of the axial R_3P-Fe-S, [**3pdt**]$^+$ = 105.11 (15)° and [**5pdt**]$^+$ = 107.93°), although the CH---Fe(1) distance does not contract further.

Small but significant differences are observed between the Fe-P distances for [**3pdt**]BF_4 and [**5pdt**]BF_4. Specifically, the Fe-P*i*-Pr_3 distance is 2.2830(15) Å, which is 0.06 Å longer than the Fe-PMe_3 distance in [**3pdt**]BF_4. The Fe-P(dppv) distances are the same in both [**3pdt**]BF_4 and [**5pdt**]BF_4. This elongated Fe-P distance is consistent with steric conjestion at this site.

Since the EPR and the crystallographic data for [**5pdt**]BF_4 do not agree, we considered the possibility that the solution structure differs from that observed in the single crystals. Indeed, an IR spectrum of a solid sample (KBr) prepared from single crystals differ distinctly from spectra for [**5pdt**]$^+$, both as a solution and as a rapidly precipitated solid (Figure 7). Significantly, the IR band at 1958 cm^{-1} for the rapidly precipitated solid is absent in the spectrum of the crystals. Furthermore, the $\nu_{\mu\text{-CO}}$ band at 1825 cm^{-1} in the rapidly precipitated material is not present in the crystalline material. When the single crystals were redissolved in CH_2Cl_2 (−45 °C), the solution IR spectrum matched that for a solution of [**5pdt**]$^+$. As a control, we demonstrated that the similarity of the IR spectra for solid (KBr) and solutions of [**3pdt**]BF_4, $\nu_{\Delta\text{-CO}} = -3$ cm^{-1} (see Supporting Information). It was not practical to compare the spectra of solution vs solid [**5edt**]BF_4, which is far less stable than [**5pdt**]BF_4.

DFT Calculations

Structures, relative stabilities, and electronic properties of different mixed valence models were studied by BP86/TZVP DFT calculations. Three families of model complexes, differing in the size of phosphine ligands, have been analyzed: $[Fe_2(S_2C_nH_{2n})(CO)_3(PH_3)_3]^+$, $[Fe_2(S_2C_nH_{2n})(CO)_3(PMe_3)(dppv)]^+$(corresponding to **[3xdt]$^+$**) and $[Fe_2(S_2C_nH_{2n})(CO)_3(Pi\text{-}Pr_3)(dppv)]^+$ (corresponding to **[5xdt]$^+$**). In each family, both edt and pdt complexes have been considered. Hereafter, the Fe atoms coordinated by one and two phosphorus ligands will be referred to as Fe^{cc} and Fe^{c}, respectively.

For $[Fe_2(S_2C_nH_{2n})(CO)_3(PH_3)_3]^+$, the lowest energy isomer (see Supporting Information) is characterized by PH_3 ligands in basal sites, and the Fecc(unrotated)-μ-C(O) distance (2.438 Å) is long. Analogous results are obtained for the $[Fe_2(S_2C_nH_{2n})(CO)_3(PMe_3)(dppv)]^+$ family (see Supporting Information), indicating that the replacement of PH_3 ligands with dppv and PMe_3 does not strongly affect the properties of the binuclear cluster. In both families ($(PH_3)_3$ and dppv-PMe_3), the energy difference between the most stable isomer and the other isomeric forms is greater for pdt than edt, due to increased steric clashing between apical P ligands and pdt. This situation is reversed when PMe_3 is replaced by P*i*-Pr_3, where the calculations suggest that rotation of Fe^{cc} and Fe^{c} are nearly isoenergetic (ΔE = 0.8 kcal/mol, Scheme 4).

In the lowest-energy [**5xdt**]$^+$ isomer, the apical vacant coordination site is located on Fe^{cc}. Moreover, relative to the corresponding $(PH_3)_3$ and (PMe_3)(dppv) cases, the μ-CO group is more symmetrically bridging. This finding is consistent with our IR data that show that $\nu_{\mu\text{-CO}}$ is 1830 cm^{-1} for [**5pdt**]$^+$ vs 1889 cm^{-1} for [**3pdt**]$^+$. The relative stability of the isomers is strongly influenced by the bulkiness of the monophosphine ligand. Steric clashing is minimized when P*i*-Pr_3 occupies a basal position trans from the basal end of the dppv chelate ring (Scheme 4, Figure 8).

Our analysis of the electronic properties of $[Fe_2(S_2C_nH_{2n})(CO)_3(PH_3)_3]^+$, $[Fe_2(S_2C_nH_{2n})(CO)_3(PMe_3)(dppv)]^+$, and $[Fe_2(S_2C_nH_{2n})(CO)_3(P\textit{i}\text{-}Pr_3)(dppv)]^+$ reveals that the unpaired electron is always localized on the iron atom featuring a vacant apical coordination position, *i.e.*, Fe^{cc} in $[Fe_2(S_2C_nH_{2n})(CO)_3(PH_3)_3]^+$ and $[Fe_2(S_2C_nH_{2n})(CO)_3(PMe_3)(dppv)]^+$, and Fecc in $[Fe_2(S_2C_nH_{2n})(CO)_3(P\textit{i}\text{-}Pr_3)(dppv)]^+$. This picture is consistent with previous DFT studies carried out on models,[7] as well as on the H-cluster.[18,19] Recent pulsed EPR analysis of the the H_{ox} state of the enzyme indicates that the unpaired electron is more localized on the non-rotated (proximal) iron.[20] This apparent discrepancy between theoretical/model and biophysical data may reflect subtle effects due to the H-cluster environment.[18] Our oxidation state assignments agree with earlier calculations by Brunold on the entire 6Fe H-cluster[19] as well as the results from Hall *et al.* on a related model containing carbene ligand on the rotated iron site.[7]

Notably, the analysis of computed partial atomic charges for $[Fe_2(S_2C_nH_{2n})(CO)_3(PH_3)_3]^+$, $[Fe_2(S_2C_nH_{2n})(CO)_3(PMe_3)(dppv)]^+$, and $[Fe_2(S_2C_nH_{2n})(CO)_3(P\textit{i}\text{-}Pr_3)(dppv)]^+$ shows that the more electrophilic metal center always corresponds to the Fe atom featuring a vacant apical coordination position (Scheme 4). Therefore, in this class of compounds, the assignment of the Fe(I) oxidation state to the iron center carrying the unpaired electron should be taken as purely formal.

Oxidation of $[Fe_2(S_2C_2H_4)(CN)(CO)_3(dppv)]^-$

We examined the oxidation of the cyanide complex $Bu_4N[Fe_2(S_2C_2H_4)(CN)(CO)_3(dppv)]$, Bu_4N[**6edt**].12 This anionic complex was expected to be more easily oxidized than the related PMe_3 derivative **3edt** and thus a potential precursor to a mixed-valence cyanide. Cyclic voltammetry indicated that this species oxidizes at −130 mV, 150 mV more cathodic than $[\mathbf{3edt}]^{0/+}$ couple. Unlike the voltammogram for the PMe_3 derivative, however, the oxidation of the cyanide was electrochemically irreversible, it re-reduces at −600 mV (ΔE_p ~ 500 mV). The *i*-V response is reminiscent of an EC process, whereby oxidation induces an irreversible chemical reaction. The CV remained unchanged even at scan rates up to 500 mV/s.

In a preparative-scale oxidation, treatment of a CH_2Cl_2 solution of Bu_4N[**6edt**] with one equiv of $FcBF_4$ afforded a thermally stable, toluene-soluble complex that proved to be diamagnetic. This species is assigned as a four-iron compound $[\mathbf{6edt}]_2$. Unlike the behavior of related phosphine complexes discussed above and elsewhere,[5,8] this oxidation was unaffected by the presence of CO, indicating the absence of long-lived unsaturated species. The corresponding two-electron oxidation of Bu_4N[**6edt**] *in MeCN solution* gives C_s-symmetric $[Fe_2(S_2C_2H_4)(\mu\text{-}CO)(CO)_2(CN)(NCMe)(dppv)]^{+}$.[12]

The ^{31}P NMR spectrum of $[\mathbf{6edt}]_2$ consisted of a broad singlet at δ 95 and a sharp singlet at δ 74.5. The low field signal is characteristic of dppv dynamically spanning apical and basal sites on diiron(I) species. A similar structure is assumed for $Fe_2(S_2C_2H_4)(CO)_4(dppv)$, which exhibits a single 31P NMR resonance at δ 94.7.[12] The sharp higher field signal is consistent with dppv on dibasal sites on diiron(II) derivatives, e.g. $[Fe_2(S_2C_2H_4)(\mu\text{-}CO)(CO)_2(PMe_3)(NCMe)(dppv)](BF_4)_2$ (δ 74.6).[12] Upon cooling the solution, each of these two signals split. The lower field signal split more, consistent with the presence of both apical and basal phosphine ligands on a diiron(I) center, whereas the splitting of the higher field signal is small (2 ppm) because the electronic asymmetry is modest, consistent with this dppv being dibasal. The IR spectrum of this charge-neutral complex resembles the sum of the spectra of $[Fe_2(S_2C_2H_4)(\mu\text{-}CO)(CO)_2(PMe_3)(MeCN)(dppv)]^{2+}$ (2058 and 2016 cm^{-1}) and the starting complex (1952 and 1901 cm^{-1}). The 1952 and 1901 cm^{-1} bands assigned to the Fe(I)-Fe(I) center occur at ~10 cm^{-1} higher energy than in Bu_4N[**6edt**], consistent with the attachment of an electrophile to the Fe*C*N. These data are consistent with the formulation $[Fe^{I}_2(S_2C_2H_4)$

$(CO)_3(dppv)](\mu\text{-}CN)[Fe^{II}_2(S_2C_2H_4)(\mu\text{-}CO)(CN)(CO)_2(dppv)]$ (Scheme 5). Further characterization of the charge-neutral product via mass spectroscopy was unsuccessful.

Discussion

Oxidation of diiron dithiolato carbonyls produces highly unsymmetrical derivatives featuring a single "rotated" iron center and a semi-bridging CO ligand. Relief of steric strain influences the regiochemistry of the oxidation, *i.e.*, the bulkier Fe center undergoes rotation. The rotation desymmetrizes the diiron center, localizing the mixed valency as indicated by EPR spectra. Addition of CO to the mixed valence species re-symmetrizes the diiron center, leading to a more delocalized mixed-valence system.[8] The central feature of these models is that the iron center that undergoes the redox-induced rearrangement remains in the Fe(I) oxidation state, whereas the iron center that undergoes oxidation remains in the same geometry and becomes coordinatively saturated. The square pyramidal iron(I) center is unsaturated and electrophilic.

Effects of Coligands on Mixed-Valency

The EPR spectra of [**2pdt**]$^+$, [**3edt**]$^+$, and [**3pdt**]$^+$ are very similar as are the crystal structures for the latter two. The rotated nature of the Fe(CO)(dppv) center was crystallographically verified for both [**3pdt**]$^+$ and [**3edt**]$^+$, and we assume that a similar structure applies to the corresponding tetracarbonyl [**2pdt**]$^+$. In face of this pattern, the EPR results are strikingly different when PMe_3 is replaced by P*i*-Pr_3 and PCy_3. Specifically, the EPR results indicate that the spin is located on the $Fe(CO)_2PR_3$ center in these bulkier complexes. The crystallography shows, however, that the Fe(CO)(dppv) remains rotated in [**5pdt**]BF_4, but we suggest that the $Fe^I(CO)_2$(P*i*-Pr_3) site is rotated in solution. DFT calculations indicate that the bulkier phosphine slightly favors rotation at the monophosphine site. P*i*-Pr_3 and PMe_3 have comparable pK_a's of ~9.7 (for PCy_3, which we assume is similar to P*i*-Pr_3) and 8.65 (PMe_3, compare 2.73 for PPh_3).20 P*i*-Pr_3 is, however, much larger than PMe_3 with a cone angle of 160° (vs 118°).21 The influence of PMe_3 vs P*i*-Pr_3 on the regiochemistry of the oxidation is also supported by the IR data as well as the electrochemical results. Compound [**5pdt**]$^+$ resembles the active site to the extent that it features two donor ligands and one CO on the "proximal" Fe center and one donor ligand and two CO's on the "distal" (rotated) Fe center (eq 3).

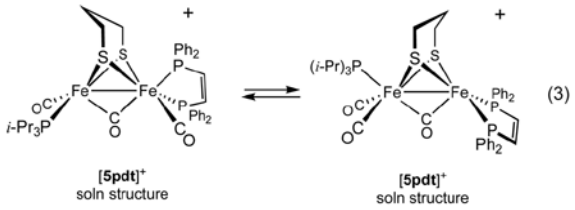

For the sake of completeness, we note that the EPR results qualitatively support two distinct descriptions, $L_3Fe^{II}(SR)_2Fe^IL_3$, which we favor,5,7,22 and $L_3Fe^{III}(SR)_2Fe^0L_3$, which has not been discussed. The 0,III description would be consistent with oxidation occurring at the more electron-rich iron center, and implies that oxidation and rotation induce a redox change at *both* iron centers, i.e., $L_3Fe^I(SR)_2Fe^IL_3 \rightarrow L_3Fe^0(SR)_2Fe^{III}L_3$. "Dative metal-metal bonds" have been invoked to describe compounds with such disparate oxidation states.[23] Precedents for ferric carbonyls include $[Cp_2Fe_2(SMe)_2(CO)_2]^{2+}$ (ν_{CO} ~ 2060 cm^{-1})[24] and the dithiocarbamate $[(C_5Me_5)Fe(S_2CNEt_2)(CO)]^+$.25 The oxidation state assignments will be further probed through studies on the Mössbauer spectra of these compounds.

Site Isolation

For low molecular weight models, a recurring question concerns the extent to which the synthetic ligands can or need to emulate the steric shielding provided by the protein. The issue is pertinent since the H-cluster is deeply imbedded in both of the structurally characterized proteins.[26] The present results highlight continuing problems that hamper the preparation of unsaturated models featuring cyanide ligands. Specifically, we showed that oxidation of a diiron cyanide leads to aggregation via formation of a μ-CN bridge. This conversion, a disproportionation, is explicable in terms of an inner sphere mechanism facilitated by the ambidentate nature of cyanide. For the present generation of models, however, tertiary phosphine ligands serve as useful surrogates for cyanide, with the advantages that their electronic and steric properties can be manipulated as we showed in this paper.

Outlook

The chemistry of mixed-valence models for the diiron active site of the [FeFe]-hydrogenases has evolved such that many details can be evaluated. For example, the nature of the dithiolate as well as the basicity and size of the coligands significantly influence the mixed valency and affect the reactivity of these species toward CO. These results will guide further efforts to understand of how substituents affect the interaction of diiron dithiolato centers toward small molecules, including H_2.

Experimental Section

Materials and methods (EPR and IR spectroscopy, and cyclic voltammetry) have recently been described.[8] $[CpFe(C_5H_4Ac)]BF_4$ was prepared by literature methods.13 The diiron complexes $Fe_2(S_2C_2H_4)(CO)_4(dppv)$, $Fe_2(S_2C_3H_6)(CO)_4(dppv)$, $Fe_2(S_2C_3H_6)(CO)_3(PMe_3)(dppv)$, $Et_4N[Fe_2(S_2C_2H_4)(CN)(CO)_3(dppv)]$ have been previously described.[12] NMR spectra were recorded at room temperature on a Varian Mercury 500 MHz spectrometer (202 MHz for ^{31}P).

X-ray Crystallography

Crystals were mounted to a thin glass fiber using Paratone-N oil (Exxon). Data, collected at 198 K on a Siemens CCD diffractometer, were filtered to remove statistical outliers. The integration software (SAINT) was used to test for crystal decay as a bi-linear function of X-ray exposure time and sin(Θ). The data were solved using SHELXTL by Direct Methods (Table 4); atomic positions were deduced from an E map or by an unweighted difference Fourier synthesis. H atom U's were assigned as $1.2U_{eq}$ for adjacent C atoms. Non-H atoms were refined anisotropically. Successful convergence of the full-matrix least-squares refinement of F^2 was indicated by the maximum shift/error for the final cycle.

EPR Spectroscopy

The following procedure is illustrative: a solution of 0.010 g (0.0116 mmol) of $Fe_2(S_2C_3H_6)(CO)_3(P\textit{i}\text{-}Pr_3)(dppv)$ in 6 mL of CH_2Cl_2 (−45 °C) was treated with a solution of 0.003 g (0.0112 mmol) of $FcBF_4$ in 6 mL of CH_2Cl_2. The resulting solution (1 mM) was transferred via cannula to a chilled (−78 °C) EPR tube that had been purged with N_2. The EPR tube was cooled with liquid nitrogen and flame-sealed under vacuum.

Spin concentrations were determined by double integrating baseline corrected spectra. For calibration, a sample containing 1 mM $CuSO_4$ in a 20% glycerol solution was recorded at the same power, modulation amplitude, and temperature as that used for the diiron samples. In this way, the spin concentration of three samples, nominally 1mM, of [**3pdt**]BF_4 were found to be 0.60, 0.60, and 0.70 mM.

DFT Calculations

DFT calculations were carried out using the BP86 functional[27] and a valence triple-ζ basis set with polarization on all atoms (TZVP).[28]

$[Fe_2(S_2C_3H_6)(CO)_4(dppv)]BF_4$ ([2pdt]BF_4)

A solution of 0.250 g (0.344 mmol) of $Fe_2(S_2C_3H_6)(CO)_4(dppv)$ in 15 mL of CH_2Cl_2 at −45 °C was treated with a solution of 0.094 g (0.344 mmol) of $FcBF_4$ in 10 mL of CH_2Cl_2. The purple solution was rapidly transferred into 400 mL of hexane cooled to −78 °C. The supernatant solvent was siphoned away from the finely divided solid. Yield: 0.152 g (54%). IR (CH_2Cl_2): ν_{CO} = 2076, 2020, 1943 cm^{-1}. IR (solid KBr): ν_{CO} = 2075, 2012, 1934, 1906 (sh) cm^{-1}.

$[Fe_2(S_2C_3H_6)(CO)_3(PMe_3)(dppv)]BF_4$ ([3pdt]BF_4)

A solution of 0.200 g (0.258 mmol) of $Fe_2(S_2C_3H_6)(CO)_3(PMe_3)(dppv)$ in 10 mL of CH_2Cl_2 at −45 °C was treated with a solution of 0.070 g (0.258 mmol) of $FcBF_4$ in 10 mL of CH_2Cl_2. The purple solution was transferred into 400 mL of hexane at −78 °C. The supernatant was removed by cannula. Crystals were grown from the liquid diffusion of hexane into a CH_2Cl_2 solution at −20 °C. Yield: 0.171 g (70%). IR (CH_2Cl_2): ν_{CO} = 2015, 1962, 1889 cm^{-1}. IR (solid KBr): ν_{CO} = 2007, 1950, 1886 cm^{-1}.

When CH_2Cl_2 solutions of [**3pdt**]BF_4 were exposed to CO (1 atm at −45 °C). The in-situ IR spectrum showed the disappearance of [**3pdt**]BF_4 and the growth of new peaks, attributed to $[Fe_2(S_2C_3H_6)(\mu\text{-}CO)(CO)_3(PMe_3)(dppv)]BF_4$, [**3pdt**CO]$BF_4$. Due to the instability of [**3pdt**CO]BF_4 all data were collected *in-situ*. IR (CH_2Cl_2): ν_{CO} = 2018, 1984, 1791 cm^{-1}. Conversion of $[\mathbf{3pdt}]^+$ to $[\mathbf{3pdt}CO]^+$ using ~1 atm CO required ~10 min.

$Fe_2(S_2C_2H_4)(CO)_3(PCy_3)(dppv)$ (4edt)

A solution of 0.300 g (0.421 mmol) of $Fe_2(S_2C_2H_4)(CO)_4(dppv)$ in 40 mL of toluene was treated with 0.130 g (0.421 mmol) of PCy_3 in 10 mL of toluene. The reaction mixture was photolyzed with a 100 W UV immersion lamp, λ_{max} = 356 nm (Spectroline), until the conversion was complete (~36 h) as indicated by IR spectroscopy. The solvent was removed in vacuum, and the product extracted into 20 mL of CH_2Cl_2. The solution was concentrated to ~5 mL, and the red-brown product precipitated upon addition of 40 mL of hexanes. Yield: 0.352 g (86 %). ^{1}H NMR (CD_2Cl_2): δ 7.98 – 7.29 (m, 20H, C_6H_5), 2.01 – 0.89 (m, 70H, P(C_6H_{22})$_3$, SCH_2CH_2S). 31P NMR (CD_2Cl_2): δ 93.96 (bs), 62.53 (s) at 20 °C. IR (CH_2Cl_2): ν_{CO} = 1953, 1901 cm^{-1}. FD-MS: m/z 964.4 ($[Fe_2(S_2C_2H_4)(CO)_3(PCy_3)(dppv)]^+$). Anal. Calcd for $C_{49}H_{59}Fe_2O_3P_3S_2$ (Found): C, 61.00 (61.38); H, 6.16 (6.50).

$[Fe_2(S_2C_2H_4)(CO)_3(PCy_3)(dppv)]BF_4$ ([4pdt]BF_4)

A solution of 0.050 g (0.052 mmol) of $Fe_2(S_2C_2H_4)(CO)_3(PCy_3)(dppv)$ in 5 mL of CH_2Cl_2 at −45 °C was treated with 14 mg (0.052 mmol) of $FcBF_4$ in 3 mL of CH_2Cl_2. IR (CH_2Cl_2): ν_{CO} = 1987 (m), 1961 (s), 1870 (br) cm^{-1}.

$Fe_2(S_2C_2H_4)(CO)_3(P\textit{i}\text{-}Pr_3)(dppv)$ (5edt)

A solution of 0.300 g (0.421 mmol) of $Fe_2(S_2C_2H_4)(CO)_4(dppv)$ in 40 mL of toluene was treated with 0.27 mL (2.105 mmol) of P*i*-Pr_3. The reaction mixture was photolyzed with a 100 W UV immersion lamp, λ_{max} = 356 nm (Spectroline) until the conversion was complete (~24 h) as indicated by IR spectra. The solvent was removed *in vacuo*, and the product was extracted into ~20 mL of CH_2Cl_2. The solution was concentrated to ~5 mL, and the red-brown product was precipitated upon addition of 40 mL of hexanes to this solution. Yield: 0.268 g (75%). ^{1}H NMR (CD_2Cl_2): δ 7.98 – 7.27 (m, 20H, C_6H_5), 2.00 (m, 3H, P(C*H*)Me_2), 1.56 (m,

2H, SCH_2), 1.26 (m, 18H, PCH(CH_3)$_2$), 1.18 (s, 2H, SCH_2). 31P NMR (CD_2Cl_2): δ 92.96 (bs), 71.74 (s) at 20 °C. 95.9 (d, $J_{P\text{-}P}$ = 25 Hz), 91.6 (d, $J_{P\text{-}P}$ = 25 Hz), 71.1 (s) at −60 °C. IR (CH_2Cl_2): ν_{CO} = 1954, 1903 cm^{-1}. FD-MS: m/z 844.4 ([$Fe_2(S_2C_2H_4)(CO)_3$(P*i*-Pr_3)(dppv)]$^+$). Anal Calcd for $C_{40}H_{47}Fe_2O_3P_3S_2$ (Found): C, 56.89 (56.97); H, 5.61 (5.45).

$Fe_2(S_2C_3H_6)(CO)_3$(P*i*-Pr_3)(dppv) (5pdt)

See preceding preparation. Yield: 71%. ^{1}H NMR (CD_2Cl_2): δ 8.00 – 7.30 (m, 20H, C_6H_5), 2.38 (m, 3H, PC*H*Me_2), 1.67 (s, 2H, SCH_2), 1.55 (s, 2H, $SCH_2CH_2CH_2S$), 1.37 (m, 18H, PCH(CH_3)$_2$), 1.25 (s, 2H, SCH_2). ^{31}P NMR (CD_2Cl_2, 20 °C): δ 90.69 (s), 72.94 (s). At −80 °C, the δ 90.69 signal is broad. IR (CH_2Cl_2): ν_{CO} = 1954, 1901 cm^{-1}. FD-MS: m/z 858.3 ([$Fe_2(S_2C_3H_6)(CO)_3$(P*i*-Pr_3)(dppv)]$^+$). Anal Calcd for $C_{41}H_{49}Fe_2O_3P_3S_2$ (Found): C, 57.36 (57.01); H, 5.75 (5.69).

[$Fe_2(S_2C_2H_4)(CO)_3$(P*i*-Pr_3)(dppv)]BF_4 ([**5edt**]BF_4)

A solution of 0.050 g (0.052 mmol) of $Fe_2(S_2C_2H_4)(CO)_3$(P*i*-Pr_3)(dppv) in 5 mL of CH_2Cl_2 at −45 °C was treated with 14 mg (0.052 mmol) of $FcBF_4$ in 3 mL of CH_2Cl_2. Due to the instability of [**5edt**]BF_4, all data were collected *in-situ*. IR (CH_2Cl_2): 3_{CO} = 1987 (m), 1968 (s), 1870 (br) cm^{-1}.

When CH_2Cl_2 solutions of [**5edt**]BF_4 were exposed to CO (1 atm at −45 °C). The in-situ IR spectrum showed the disappearance of [**5edt**]BF_4 and the growth of new peaks, attributed to [$Fe_2(S_2C_3H_6)$(μ-CO)$(CO)_3$(P*i*-Pr_3)(dppv)]BF_4, [**5edt**CO]BF_4. Due to the instability of [**5edt**CO]BF_4, all data were collected *in-situ*. IR (CH_2Cl_2): ν_{CO} = 2022, 1987, 1968, 1787 cm^{-1}. The reaction of CO with [**5edt**]$^+$ to form [**5edt**CO]$^+$ required ~30 min.

[$Fe_2(S_2C_3H_6)(CO)_3$(P*i*-Pr_3)(dppv)]BF_4 ([**5pdt**]BF_4)

A solution of 0.150 g (0.175 mmol) of $Fe_2(S_2C_3H_6)(CO)_3$(P*i*-Pr_3)(dppv) in 20 mL of CH_2Cl_2 at −45 °C was treated with 0.047 mg (0.175 mmol) of $FcBF_4$ in 10 mL of CH_2Cl_2. The solution was transferred via cannula to 400 mL of hexane cooled to −78 °C to precipitate the red-brown solid. Single crystals were grown by diffusion of a layer of hexane into a CH_2Cl_2 solution at −20 °C. IR (CH_2Cl_2): ν_{CO} = 2011 (sm), 1988 (m), 1968 (s), 1830 (br) cm^{-1}. IR of rapidly precipitated solid (KBr): ν_{CO} = 1998 (m), 1958 (s), 1904 (sm), 1824 (br) cm^{-1}. IR of pulverized single crystals (KBr): ν_{CO} = 1990 (s), 1931 (s), 1903 (m) cm^{-1}.

[$Fe_2(S_2C_2H_4)(CN)(CO)_3$(dppv)]$_2$ ([**6edt**]$_2$)

A solution of 0.050 g (0.0525 mmol) of Bu_4N[$Fe_2(S_2C_2H_4)(CN)(CO)_3$(dppv)] in 5 mL of CH_2Cl_2 was treated with 0.014 g (0.0525 mmol) of $FcBF_4$ in 5.0 mL of CH_2Cl_2. Solvent was removed in vacuo, and the product was extracted into 20 mL of toluene. The orange solution was concentrated to 5 mL, and the product precipitated upon addition of 30 mL of hexanes. ^{31}P NMR (CD_2Cl_2, 20 °C): δ 92.96 (bs), 71.74 (s). ^{31}P NMR (CD_2Cl_2, −60 °C): 99.1 (d, $J_{P\text{-}P}$ = 21 Hz), 92.7 (d, $J_{P\text{-}P}$ = 21 Hz), 75.9 (s), 74.0 (s). IR (CH_2Cl_2): ν_{CN} = 2136, 2116 cm^{-1}. IR (CH_2Cl_2): ν_{CO} = 2074 (sh), 2058 (s), 2016 (m), 1975 (m), 1952 (s), 1901 (s) cm^{-1}.

Acknowledgements

This research was supported by NIH.

References

1. Liu X, Ibrahim SK, Tard C, Pickett CJ. Coord Chem Rev 2005;249:1641–1652.Tard C, Liu X, Ibrahim SK, Bruschi M, De Gioia L, Davies SC, Yang X, Wang LS, Sawers G, Pickett CJ. Nature 2005;433:610–4. [PubMed: 15703741]

2. De Lacey AL, Fernández VM, Rousset M, Cammack R. Chem Rev 2007;107:4304–4330. [PubMed: 17715982]Fontecilla-Camps JC, Volbeda A, Cavazza C, Nicolet Y. Chem Rev 2007;107:4273–4303. [PubMed: 17850165]
3. Lubitz W, Reijerse E, van Gastel M. Chem Rev 2007;107:4331–4365. [PubMed: 17845059]Vignais PM, Billoud B. Chem Rev 2007;107:4206–4272. [PubMed: 17927159]
4. Liu T, Darensbourg MY. J Am Chem Soc 2007;129:7008–9. [PubMed: 17497786]
5. Justice AK, Rauchfuss TB, Wilson SR. Angew Chem, Int Ed 2007;46:6152–6154.
6. Justice AK, Zampella G, De Gioia L, Rauchfuss TB. Chem Commun 2007:2019–21.
7. Thomas CM, Darensbourg MY, Hall MB. J Inorg Biochem 2007;101:1752–1757. [PubMed: 17698202]
8. Justice AK, Nilges M, De Gioia L, Rauchfuss TB, Wilson SR, Zampella G. J Am Chem Soc 2008;130:5293–5301. [PubMed: 18341276]
9. Schmidt M, Contakes SM, Rauchfuss TB. J Am Chem Soc 1999;121:9736–7.Lyon EJ, Georgakaki IP, Reibenspies JH, Darensbourg MY. Angew Chem, Int Ed Engl 1999;38:3178–3180. [PubMed: 10556894]Le Cloirec A, Davies SC, Evans DJ, Hughes DL, Pickett CJ, Best SP, Borg S. Chem Commun 1999:2285–2286.
10. Zhao X, Georgakaki IP, Miller ML, Yarbrough JC, Darensbourg MY. J Am Chem Soc 2001;123:9710–9711. [PubMed: 11572707]Razavet M, Borg SJ, George SJ, Best SP, Fairhurst SA, Pickett CJ. Chem Commun 2002:700–701.
11. Boyke CA, van der Vlugt JI, Rauchfuss TB, Wilson SR, Zampella G, De Gioia L. J Am Chem Soc 2005;127:11010–11018. [PubMed: 16076208]
12. Justice AK, Zampella G, De Gioia L, Rauchfuss TB, van der Vlugt JI, Wilson SR. Inorg Chem 2007;46:1655–1664. [PubMed: 17279743]
13. Connelly NG, Geiger WE. Chem Rev 1996;96:877–922. [PubMed: 11848774]
14. Olsen MT, Justice AK, Rauchfuss TB, Wilson SR. in preparation
15. Boyke CA, Rauchfuss TB, Wilson SR, Rohmer MM, Bénard M. J Am Chem Soc 2004;126:15151–15160. [PubMed: 15548012]
16. MacNeil JH, Chiverton AC, Fortier S, Baird MC, Hynes RC, Williams AJ, Preston KF, Ziegler T. J Am Chem Soc 1991;113:9834–9842.Baker PK, Connelly NG, Jones BMR, Maher JP, Somers KR. J Chem Soc, Dalton Trans 1980:579–585.And references therein
17. Brookhart M, Green MLH, Parkin G. Proc Natl Acad Sci 2007;104:6908–14. [PubMed: 17442749]
18. To probe the possibility that the spin could reside on the non-rotated site, we have carried out time-dependent DFT calculations on $[Fe_2(S_2C_nH_{2n})(CO)_3(PH_3)_3]^+$, evaluating the possible presence of low-lying excited states in which the unpaired electron is not localized on the Fe atom featuring vacant apical coordination site. We found that the lowest-energy excited state is about 23 kcal/mol higher in energy than the ground state. More importantly, in the excited state the spin density distribution was largely unaffected.
19. Fiedler AT, Brunold TC. Inorg Chem 2005;44:9322–9334. [PubMed: 16323916]
20. Bush RC, Angelici RJ. Inorg Chem 1988;27:681–686.
21. Tolman CA. Chem Rev 1977;77:313–48.
22. Silakov A, Reijerse EJ, Albracht SPJ, Hatchikian EC, Lubitz W. J Am Chem Soc 2007;129:11447–11458. [PubMed: 17722921]
23. Jiang F, Jenkins HA, Biradha K, Davis HB, Pomeroy RK, Zaworotko MJ. Organometallics 2000;19:5049–5062.Jiang F, Biradha K, Leong WK, Pomeroy RK, Zaworotko MJ. Can J Chem 1999;77:1327–1335.
24. de Beer JA, Haines RJ, Greatrex R, van Wyk JA. J Chem Soc, Dalton Trans 1973:2341.Vergamini PJ, Kubas GJ. Prog Inorg Chem 1976;21:261–82.Madec P, Muir KW, Pétillon FY, Rumin R, Scaon Y, Schollhammer P, Talarmin J. J Chem Soc Dalton Trans 1999:2371–2384.
25. Delville-Desbois MH, Mross S, Astruc D, Linares J, Varret F, Rabaâ H, Le Beuze A, Saillard JY, Culp RD, Atwood DA, Cowley AH. J Am Chem Soc 1996;118:4133–47.
26. Pandey AS, Harris TV, Giles LJ, Peters JW, Szilagyi RK. J Am Chem Soc 2008;130:4533–4540. [PubMed: 18324814]Nicolet Y, Lemon BJ, Fontecilla-Camps JC, Peters JW. Trends Biochem Sci 2000;25:138–143. [PubMed: 10694885]

27. Becke AD. J Chem Phys 1986;84:4524–4529.Perdew JP. Phys Rev 1986;B33:8882.
28. Schaefer A, Huber C, Ahlrichs R. J Chem Phys 1994;100:5829–35.

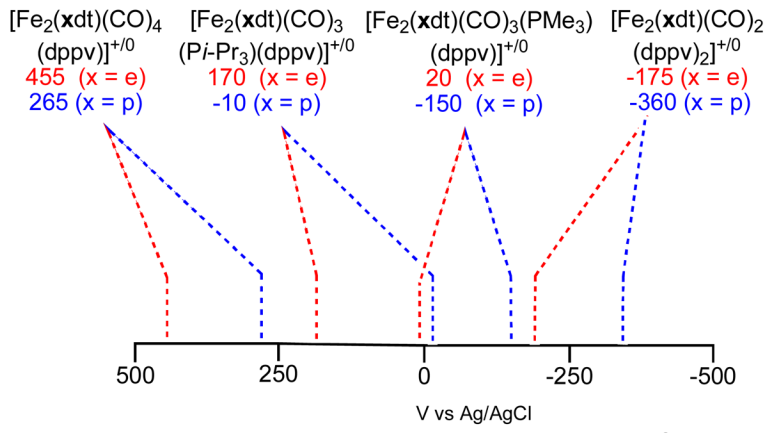

Figure 1.

Redox properties of diiron(I) dithiolates (CH_2Cl_2 soln).[a]

[a]Unless indicated otherwise, couples are reversible as judged from the finding that i_{pc}/i_{pa} ~1.

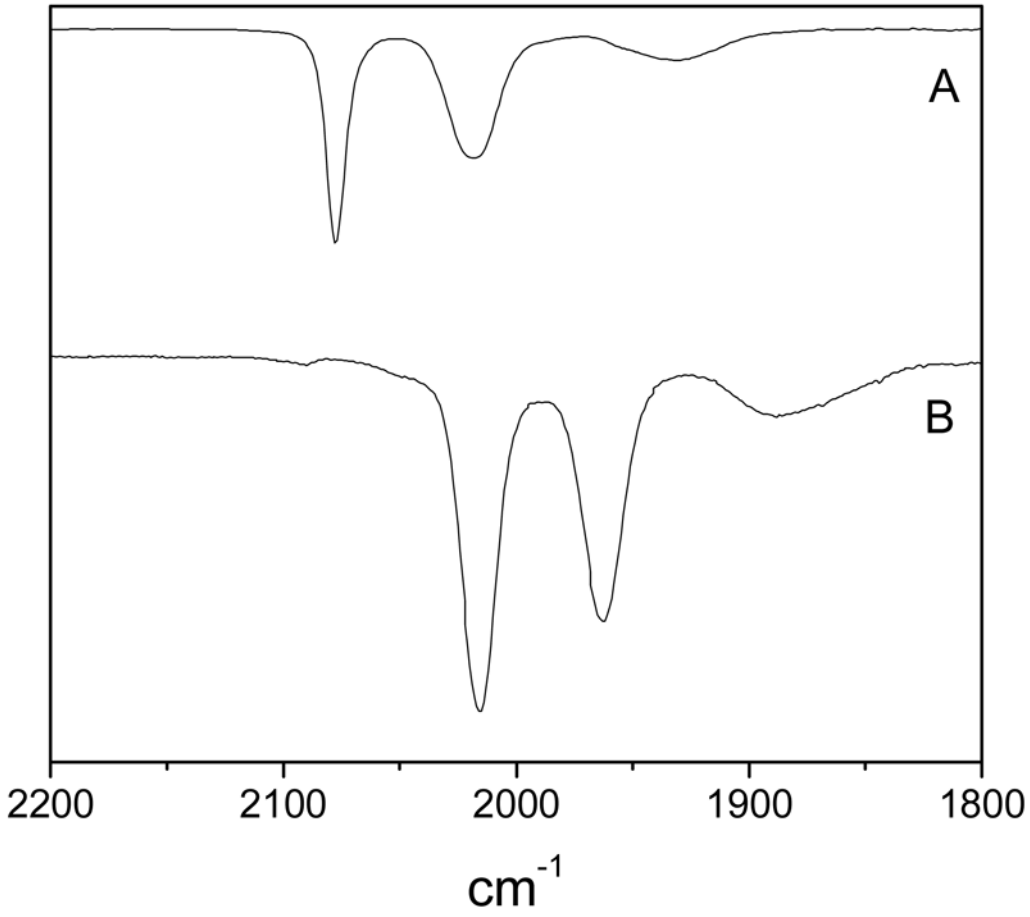

Figure 2.
IR spectra (CH_2Cl_2 solns) of $[Fe_2(S_2C_3H_4)(CO)_4(dppv)]BF_4$ ([**2pdt**]BF_4, A) and $[Fe_2(S_2C_3H_6)(CO)_3(PMe_3)(dppv)]BF_4$ ([**3pdt**]BF_4, B).

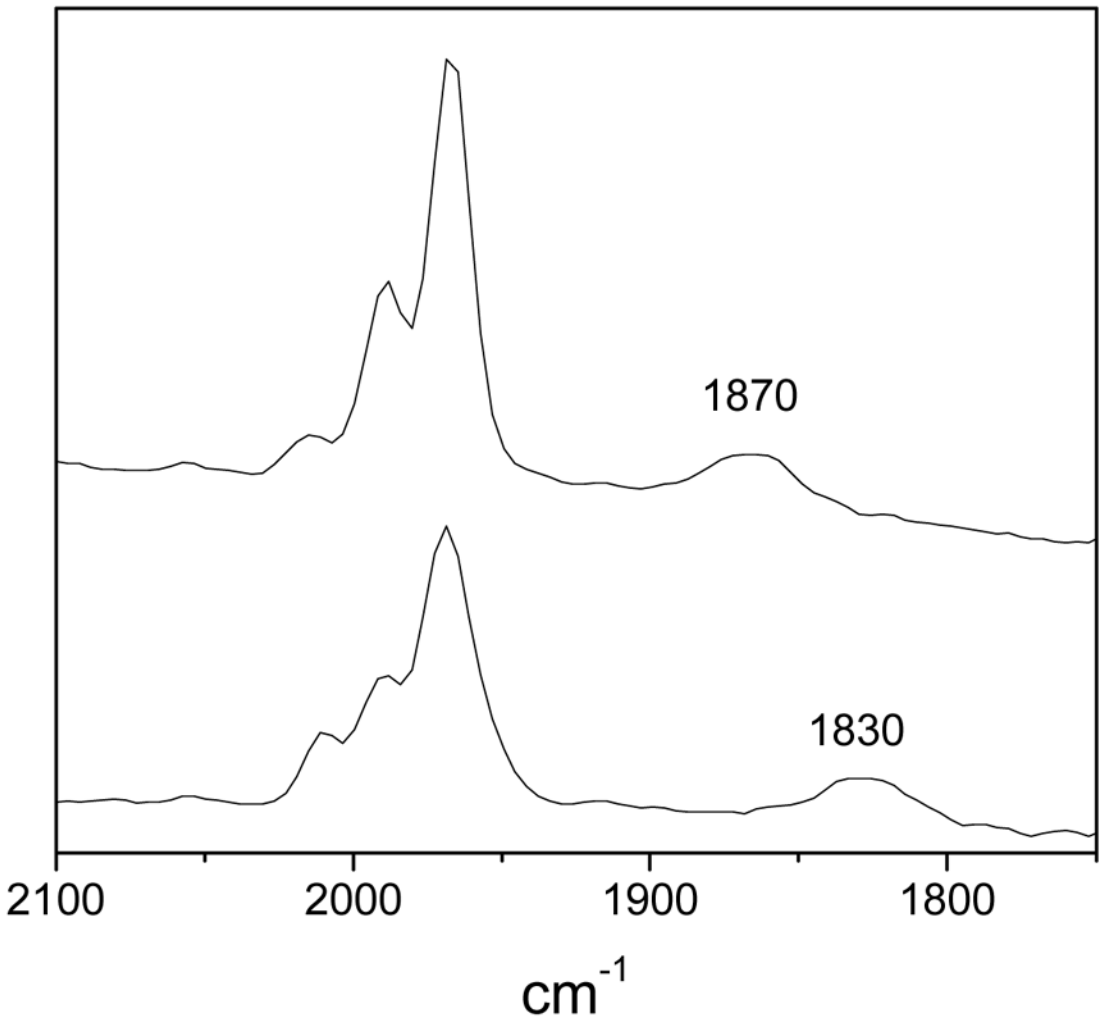

Figure 3.
IR spectra (absorbance mode, CH_2Cl_2 at −45 °C) showing the effects of edt vs pdt for the oxidation of complexes containing bulky phosphine ligands: $[Fe_2(S_2C_2H_4)(CO)_3(P\textit{i}\text{-}Pr_3)(dppv)]BF_4$ ([**5edt**]BF_4, top) and $[Fe_2(S_2C_3H_6)(CO)_3(P\textit{i}\text{-}Pr_3)(dppv)]BF_4$ ([**5pdt**]BF_4, bottom).

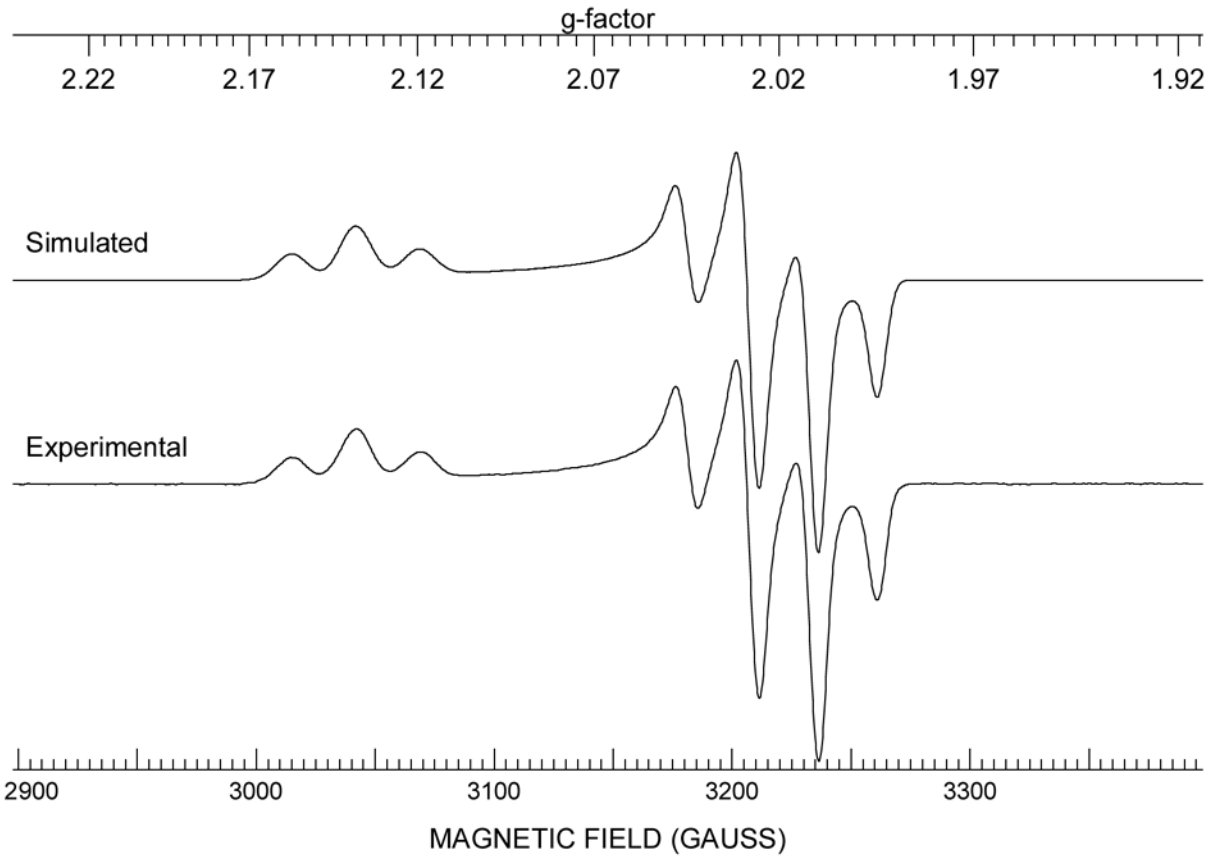

Figure 4.
X-Band EPR spectra (110K, 1:1 CH_2Cl_2: toluene frozen solution) of $[Fe_2(S_2C_2H_4)(CO)_3(PMe_3)(dppv)]BF_4$ ([**3edt**]BF_4). Top is the simulation and bottom is experimental data.

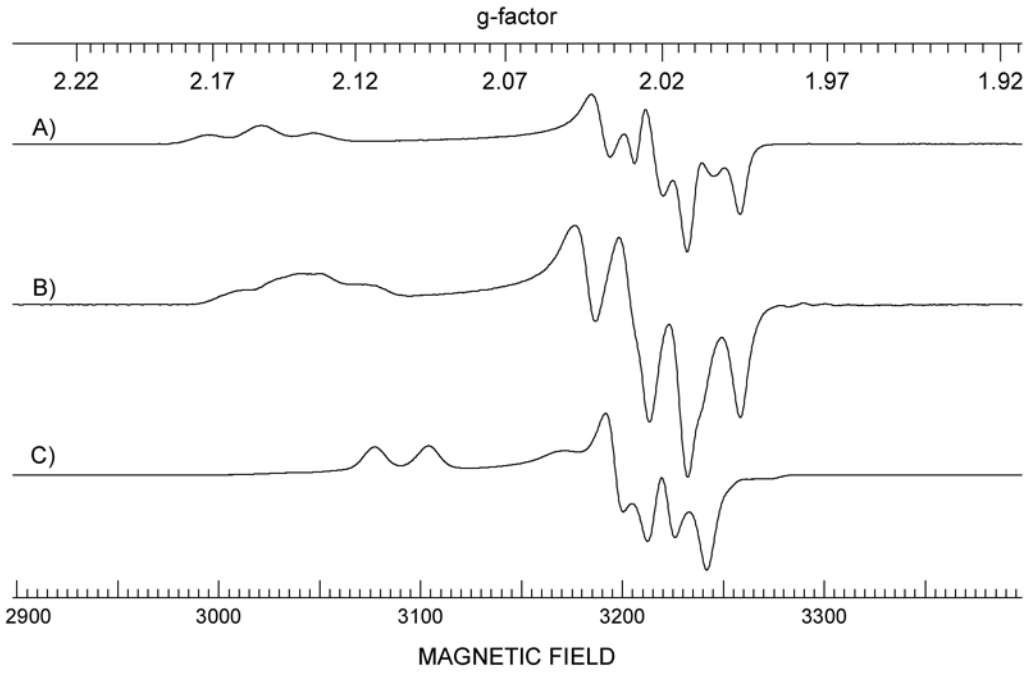

Figure 5.
X-Band EPR spectra (110K, 1:1 CH_2Cl_2:toluene frozen solution): $[Fe_2(S_2C_3H_6)(CO)_4(dppv)]^+$ ([**2pdt**]$^+$, a), $[Fe_2(S_2C_3H_6)(CO)_3(PMe_3)(dppv)]^+$ ([**3pdt**]$^+$, b), $[Fe_2(S_2C_3H_6)(CO)_3(P\textit{i}\text{-}Pr_3)(dppv)]^+$ ([**5pdt**]$^+$, c).

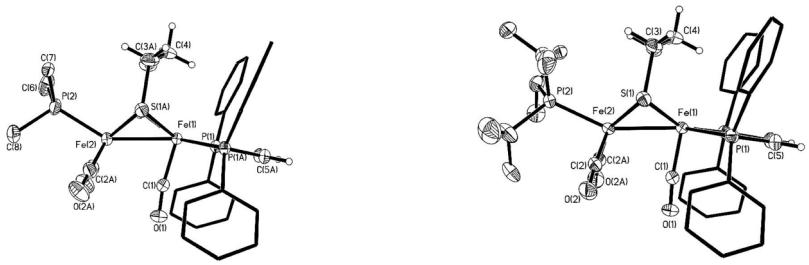

Figure 6.
Structure of the cations in [**3pdt**]BF_4 and [**5pdt**]$BF_4$with thermal ellipsoids set at 35% level. Phenyl ellipsoids, hydrogen atoms, and the BF_4^- were omitted for clarity.

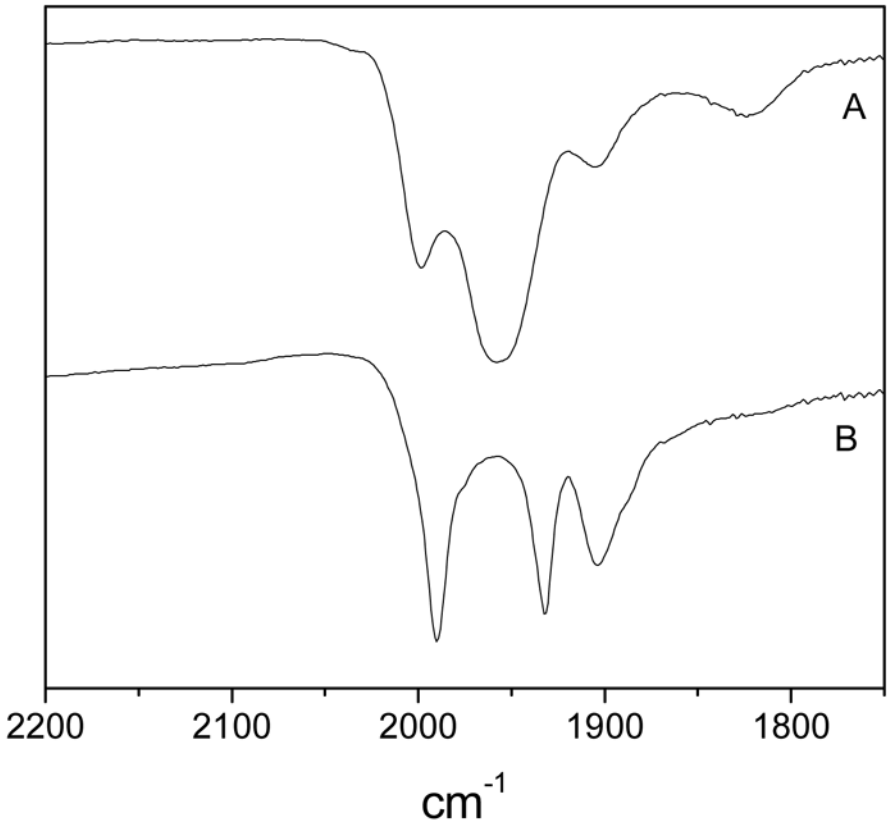

Figure 7.
IR spectra (KBr) of [**5pdt**]BF_4 that was rapidly precipitated (top) and single crystals grown at −20 °C (bottom).

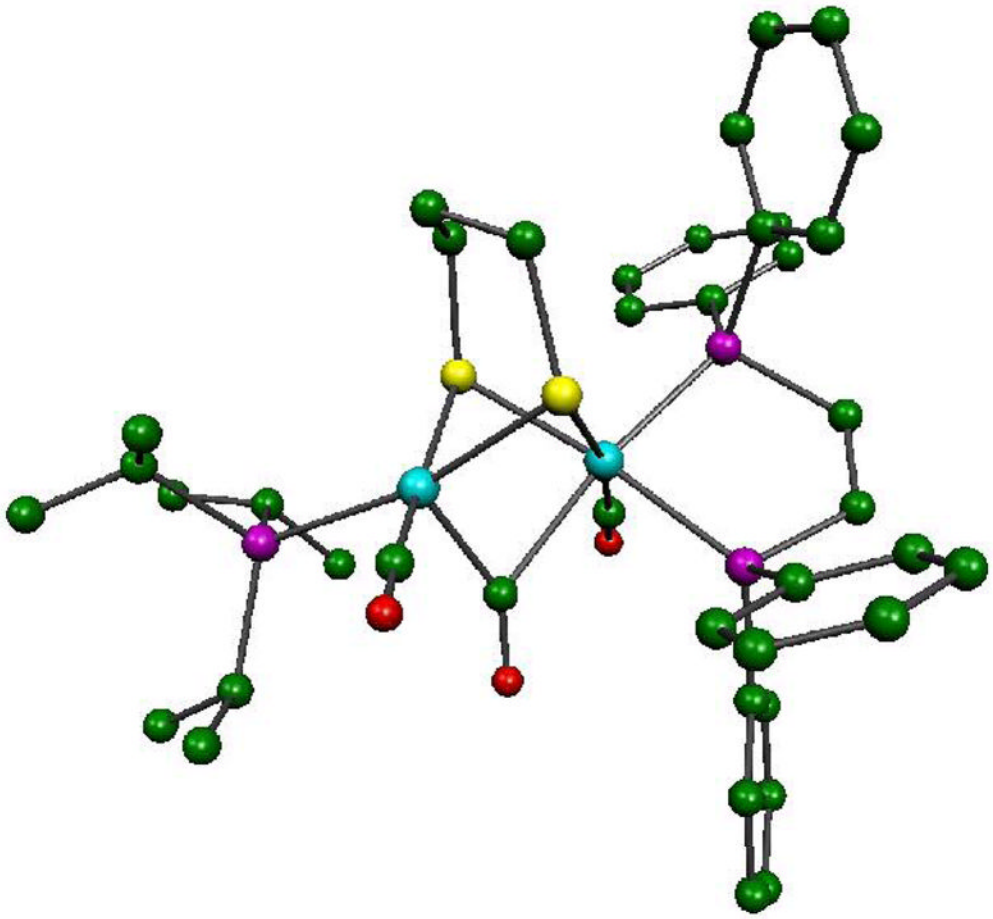

Figure 8.
DFT structure of the lowest energy isomer of $[Fe_2(S_2C_3H_6)(CO)_3(P\textit{i}\text{-}Pr_3)(dppv)]^+$ ($[5pdt]^+$). Atoms are color coded as follows: carbon, green; oxygen, red; sulfur, yellow; phosphorus, purple; iron, cyan.

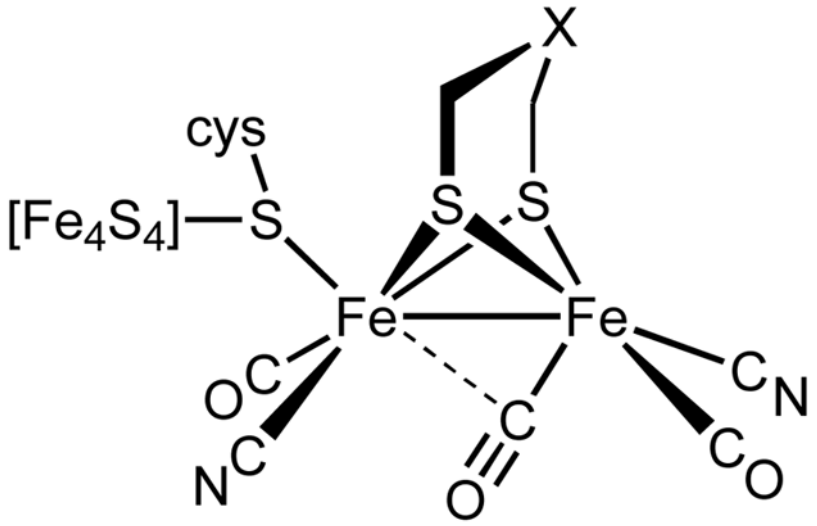

Scheme 1.
Structure of the diiron active site of the H_{ox} state of the [FeFe]-hydrogenases (X is CH_2, NH, or O).

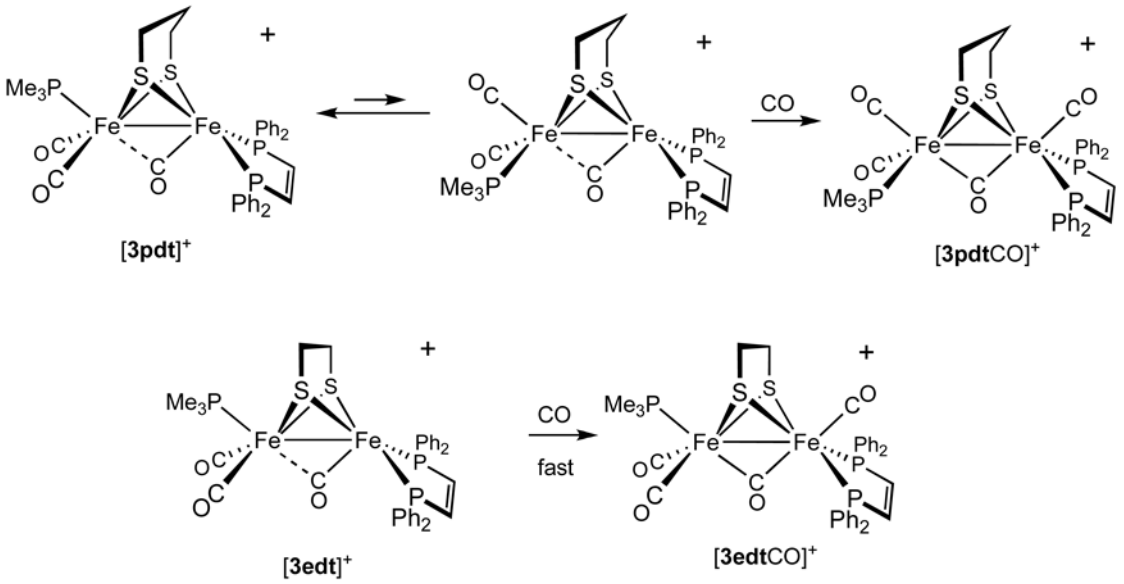

Scheme 2.
Pathways for the carbonylations of [**3edt**]$^{+}$ and [**3pdt**]$^{+}$.

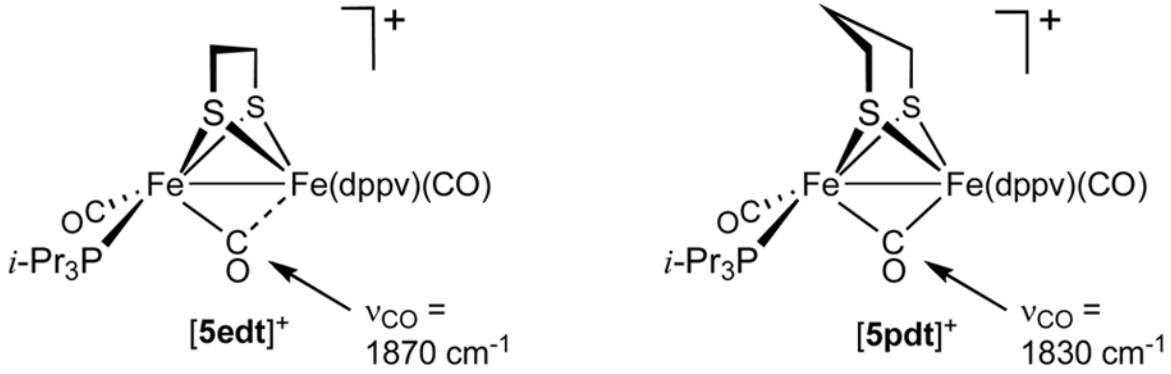

Scheme 3.
Proposed solution structures of [**5edt**]$^{+}$ and [**5pdt**]$^{+}$.

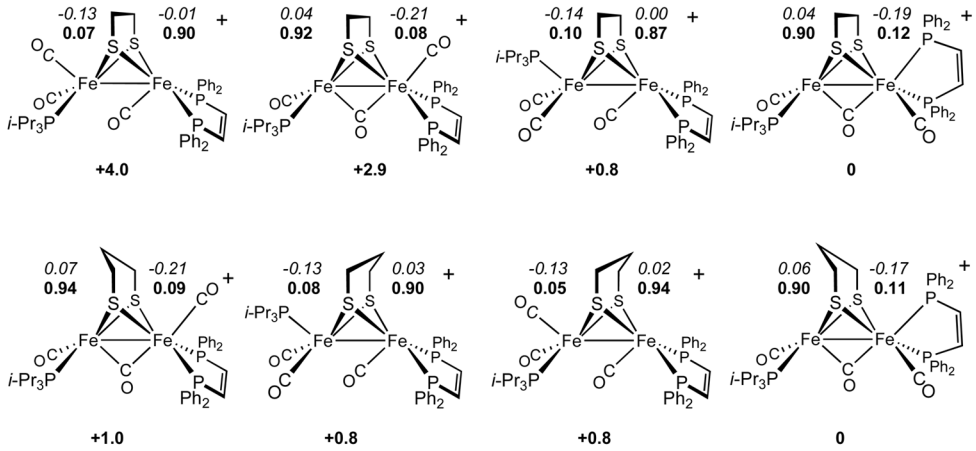

Scheme 4.

Computed relative stabilities (kcal/mol), spin densities, and NBO partial atomic charges (*italics*) for relevant isomers of $[Fe_2(S_2C_nH_{2n})(CO)_3(P\textit{i}\text{-}Pr_3)(dppv)]^+$.

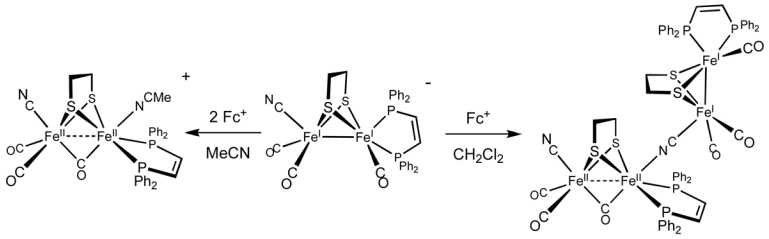

Scheme 5.
Redox reactivity proposed for $[Fe_2(S_2C_2H_4)(CN)(CO)_3(dppv)]^{-}$.

Table 1

Selected EPR Parameters for $[Fe_2(S_2C_XH_{2X})(CO)_2L(dppv)]BF_4$ (Spectra Recorded at 110 K (−163 °C), in 1:1 CH_2Cl_2:toluene).

Complex (donor ligands)	g_z	A_{zz}	g_y	A_{yy}	g_x	A_{xx}
[**2pdt**]$^+$ (dppv)	2.1490	78, 78	2.0199	71, 71	2.0086	72, 72
[**3edt**]$^+$ (dppv, PMe_3)	2.1384	80, 80	2.0280	74, 74	2.0102	72, 72
[**3pdt**]$^{+a}$ (dppv, PMe_3)	2.1310 2.1410	82, 82 81, 81	2.0223 2.0268	76, 76 73, 73	2.0085 2.0064	74, 74 75, 75
[**4edt**]$^+$ (dppv, PCy_3)	2.0958	69	2.0423	67	2.0098	73
[**5edt**]$^+$ (dppv, P*i*-Pr_3)	2.0968	70	2.0437	71	2.0105	75
[**5pdt**]$^+$ (dppv, P*i*-Pr_3)	2.1046	80	2.0268	73	2.0149	80

^{a}For [**3pdt**]$^+$ the two species are present in at 2:1 ratio.

Table 2

Selected EPR Parameters for $[Fe_2(S_2C_xH_{2x})(\mu\text{-}CO)(CO)_3L(dppv)]BF_4$ (Spectra Recorded at 110K (−163 °C), in 1:1 CH_2Cl_2:toluene)

Complex	g_z	A_{zz}	g_y	A_{yy}	g_x	A_{xx}
[**3edt**CO]$^+$	1.9943	323, 39, 42	1.9740	263, 28, 30	2.0073	258, 30, 33
[**3pdt**CO]$^+$	1.9976	30, 40, 36	1.9814	24, 30, 26	2.0131	24, 31, 26
[**5edt**CO]$^+$	1.9939	313, 36, 33	1.9750	254, 30, 28	2.0075	255, 27, 27

Table 3

Selected Structural Parameters for $[Fe_2(S_2C_3H_6)(CO)_3L(dppv)]BF_4$ (L = PMe_3, P*i*-Pr_3).

Distances (Å)	L = P*i*-Pr_3	L = PMe_3	Angles (deg.)	L = P*i*-Pr_3	L = PMe_3
Fe(1)–Fe(2)	2.5824 (10)	2.5768 (8)	Fe(1)–S(1)–Fe(2)	69.53 (3)	69.53(3)
Fe(1)–S(1)	2.2745 (10)	2.2730 (8)	Fe(1)–Fe(2)–S(1)	55.60 (3)	55.73 (2)
Fe(2)–S(1)	2.2544 (11)	2.2460 (8)	Fe(2)–Fe(1)–S(1)	54.87 (3)	54.74 (2)
Fe(1)–C(1)	1.785 (5)	1.786 (4)	Fe(2)–Fe(1)–C(1)	78.55 (16)	73.20 (13)
Fe(2)–C(1)	2.833	2.678	Fe(2)–Fe(1)–P(1)	136.39 (3)	135.44 (2)
Fe(1)–P(1)	2.2387 (11)	2.2369 (8)	P(1)–Fe(1)–C(1)	92.15 (12)	93.86 (10)
Fe(2)–C(2)	1.774 (4)	1.787 (3)	Fe(1)–Fe(2)–C(2)	103.25 (13)	108.92 (10)
Fe(2)–P(2)	2.2830 (15)	2.2273 (15)	Fe(1)–Fe(2)–P(2)	154.09 (5)	147.79 (5)
C(1)–O(1)	1.147 (6)	1.148 (5)	P(2)–Fe(2)–C(2)	94.63 (13)	94.37 (18)
C(2)–O(2)	1.139 (5)	1.142(4)	C(2) –Fe(2)–C(2A)	91.9 (3)	93.0 (2)
			Fe(1)–C(1)–O(1)	173.0 (5)	171.2 (4)
			Fe(2) –C(2)–O(2)	175.8 (4)	177.8 (3)

Table 4

Details of Data Collection and Structure Refinement for Crystallography.

Complex	**[3pdt]BF_4**	**[5pdt]BF_4**
Chemical formula	$C_{35}H_{37}BF_4Fe_2O_3P_3S_2$	$C_{41}H_{49}BF_4Fe_2O_3P_3S_2$
Temperature (K)	193 (2)	193 (2)
Crystal size (mm^3)	0.28 × 0.12 × 0.06	0.31 × 0.08 × 0.08
Crystal system	Orthorhombic	Monoclinic
Space group	Pnma	$P2_1/m$
a (Å)	23.5362 (7)	9.2644 (7)
b (Å)	18.3985 (5)	16.1182 (12)
c (Å)	8.5950 (2)	16.1141 (12)
α(°)	90	90
β(°)	90	105.462 (2)
γ(°)	90	90
V ($Å^3$)	3721.90 (17)	2319.2 (3)
Z	4	2
Density calcd (Mg m^{-3})	1.537	1.475
μ(Mo K_α, mm^{-1})	0.71073	0.71073
max./min. trans'n	0.9422/0.8116	0.9323/0.7729
reflections meas'd/Indep.	47014/3695	27790/4544
data/restraints/parameters	3695/261/339	4544/503/471
GOF on F^2	1.083	1.069
Rint	0.0623	0.0431
R1 [I > 2σ] (all data)[a]	0.0380 (0.0552)	0.0505 (0.0642)
wR2 [I > 2σ] (all data)[b]	0.0904 (0.1003)	0.1328 (0.1414)
max. peak/hole ($e^-/Å^3$)	0.715/−0.322	1.036/−0.548

[a] $R1 = \Sigma||F_O|-|F_C||/\Sigma|F_O|$

[b] $wR2 = \{[w(|F_O|-|F_C|)^2]/\Sigma[wF_O^2]\}^{1/2}$, where $w = 1/\sigma^2(F_O)$